Modeling Azimuth Ambiguities in Focused SAR Data

Naomi Petrushevsky[a] and Andrea Monti-Guarnieri[a]
[a]Politecnico di Milano, Department of Electronics, Information and Bioengineering, Via Ponzio 34/5, 20133 Milan, Italy.

Abstract

Azimuth ambiguities are an intrinsic characteristic of a Synthetic Aperture Radar (SAR) image caused by aliasing of the Doppler spectrum. This work presents a complete 2D model of the replica's structure regarding power distribution and phase pattern. It is shown that the false target is a smeared version of the true signal, and the dispersion is well predicted by a closed-form model. A deep understanding of such features can assist in retrieving the true signal superposed by aliasing or even in using azimuth ambiguities as an additional source of information. The model was validated by simulation and a real COSMO-SkyMed acquisition. By considering the derived model, it was possible to refocus the ambiguous regions and recover the original targets.

1 Introduction

A Synthetic Aperture Radar (SAR) system emulates a wide antenna in the azimuth direction by periodically sampling the scene as the sensor moves along its trajectory. The Pulse Repetition Frequency (PRF) defines the observed Doppler bandwidth, and any higher frequencies are folded into the main signal. The result of the aliasing is azimuth ambiguities, i.e., the appearance of false replicas in the final image.

While the antenna pattern somewhat attenuates azimuth ambiguities, they are known to degrade the SAR image, as the true backscatter is overlapped with undesired ghost signal [1]. Many studies have demonstrated the detection of such disturbances by using, for example, their spectral [2] and polarimetric [3] properties. Moreover, in certain conditions, removing strong replicas is possible [4, 5].

The power of azimuth ambiguities has always been an essential measure of SAR imaging quality. The recent growing interest in formations of small SAR satellites [6] makes the study of aliasing especially relevant, as each sensor down-samples the scene and generates a highly ambiguous image. Precise modeling of the replica's structure can improve its suppression or enable its usage as an additional signal.

In this paper, we propose to deepen the understanding of the ambiguity's structure by devising its complete 2D Impulse-Response Function (IRF). While the ambiguous signal originates from some true target, it is not a precise copy because it stems from a different Doppler centroid [7]. Many studies have discussed important characteristics of azimuth ambiguities [8, 7], but a complete 2D model was not yet presented, to the best of our knowledge. The provided description of ambiguities in a focused SAR image accounts for both amplitude and phase.

The model was validated by simulated data and a real COSMO-SkyMed acquisition. The latter mission was designed to have a sufficiently low Azimuth Ambiguity to Signal Ratio (AASR) [9], so the replicas are generally not visible and merely contribute to an elevated level of clutter noise. However, we have observed several strong scatterers which generate significant replicas. Such disturbances in a standard acquisition highlight the importance of studying and controlling ambiguities.

1.1 The Aliased Spectrum

For small apertures and small range intervals, the transformed monostatic acquisition phase operator can be approximated by [10]:

$$H_s(k_r, k_x, r_0) = \exp\left(j \frac{r_0}{2\Omega_0}\left(k_x^2 - \frac{k_x^2\,(k_r - \Omega_0)}{\Omega_0}\right)\right) \quad (1)$$

where k_x and k_r are the azimuth and slant-range angular frequencies, respectively. r_0 is the zero-doppler distance, and $\Omega_0 = 4\pi/\lambda$, λ being the wavelength of the carrier. The following analysis considers a zero squint; however, it can be easily extended to account for geometries with higher squint.

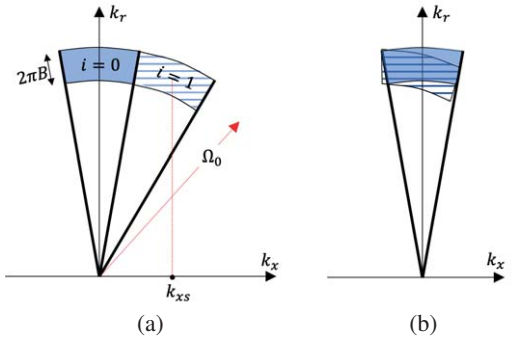

Figure 1 Representation of the spectrum of a point target (uniformly shaded) with its first ambiguous part (filled with line pattern): (a) Unfolded spectrum, showing the two parts side by side. (b) Actual spectrum, where angular frequencies above $k_{xs}/2$ are folded into the main signal.

ISBN 978-3-8007-6286-6 / ISSN 2197-4403

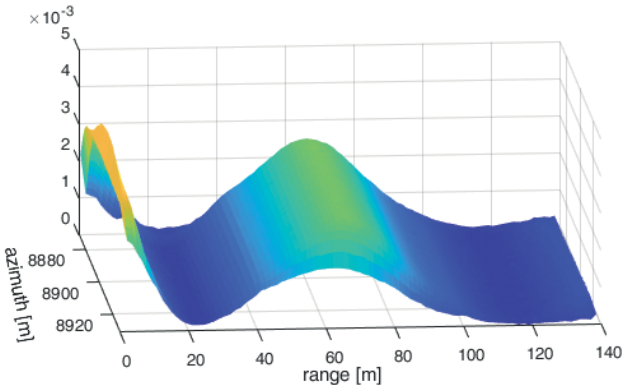

Figure 2 Amplitude of the defocused ambiguity. The azimuth antenna pattern determines the amplitude along the slant-range direction.

The PRF of a SAR system defines the azimuth bandwidth:

$$|k_x| \leq \frac{\pi}{v_s} PRF = \frac{k_{xs}}{2} \tag{2}$$

where v_s is the spacecraft's along-track (AT) velocity, and k_{xs} denotes the sampling angular frequency. For frequencies above the limit defined above, the spectrum is repeated periodically. In practice, the range of angles observed by the synthetic aperture is much larger, causing high-frequency components to fold into the main spectrum, as shown in Fig.1. The antenna pattern attenuates the amplitude of such folds, following the sinc-squared approximation:

$$G_a(k_x) \approx \text{sinc}^2\left(\frac{L_a}{4\pi} k_x\right) \tag{3}$$

where L_a is the length of the antenna.
By combining (1) and (3) we can express the aliased spectrum of the range-compressed data within the range of frequencies defined in (2):

$$U(k_r, k_x) = \sum_i G_a(k_x + ik_{xs}) \cdot H_s(k_r, k_x + ik_{xs}) \tag{4}$$

being i the index of the fold.
The appearance of a false target in the final image is caused by focusing the aliased signal (4) with the operator that is phase-matched to the expression in (1). The spectrum of the focused ambiguity i can be expressed as:

$$S_i(k'_r, k_x) = G_a(k_x + ik_{xs}) e^{j\phi_i(k'_r, k_x)} \tag{5}$$

Table 1 Parameters of the simulated acquisition.

Parameter	Description	Value
λ	wavelength	3.12cm
L_a	antenna length	3m
r_0	slant-range	570km
PRF	pulse repetition frequency	7500Hz
v_s	satellite AT velocity	7500m/s
B	range bandwidth	60MHz

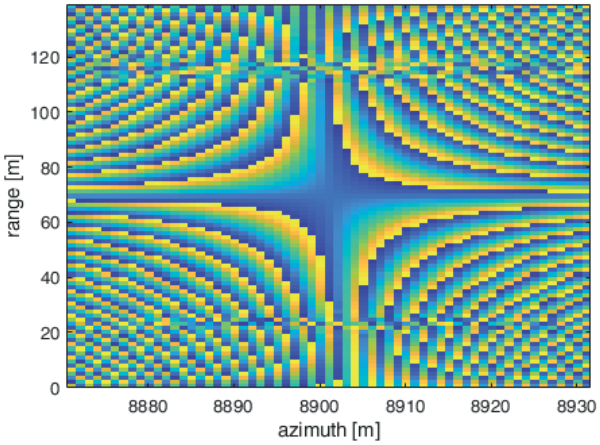

Figure 3 The phase of a defocused ambiguity, described by a hyperbolic paraboloid.

$$\phi_i(k'_r, k_x) = \frac{r_0}{2\Omega_0}\left[(ik_{xs})^2 + 2ik_{xs}k_x - \frac{(ik_{xs})^2}{\Omega_0}k'_r - \frac{2ik_{xs}}{\Omega_0}k'_r k_x\right] \tag{6}$$

where $k'_r = k_r - \Omega_0$. The first term in the residual phase ϕ_i is the extra path caused by the different Doppler centroid. It is a pure phase contribution proportional to the slant-range and the sampling frequency. The second and third components are the well-known displacements of the replica in azimuth (Δx_i) and range (Δr_i) [8]:

$$\Delta x_i = -\frac{r_0 \lambda}{2dx} i \tag{7}$$

$$\Delta r_i = \frac{(\Delta x_i)^2}{2r_0} \tag{8}$$

where dx is the azimuth sampling interval in meters.
The last term of (6) accounts for the defocusing of the ambiguity, i.e., it's spread over several pixels. The analysis of the defocusing term is the main contribution of this work.

2 Ambiguity IRF

This section formulates the complete 2D IRF of an azimuth ambiguity. The defocusing operator is analyzed first, starting from its spectrum from (5) and (6):

$$S_{i,def}(k'_r, k_x) = G_a(k_x + ik_{xs}) e^{-jaik'_r k_x} \tag{9}$$

where $a = r_0 k_{xs}/\Omega_0^2$. The 2D structure of an ambiguity in the focused data can be derived by back-transforming (9):

$$s_{i,def}(r, x) = \frac{1}{4\pi^2} \int_{-\frac{\pi}{dx}}^{\frac{\pi}{dx}} \int_{-\frac{\pi}{\rho}}^{\frac{\pi}{\rho}} G_a(k_x + ik_{xs}) e^{-jaik'_r k_x} e^{jk_x x} e^{jk'_r r} dk'_r dk_x \tag{10}$$

where $\rho = c/2B$, i.e., the slant range resolution. The evaluation of the integral above can be carried out in two steps: by first assuming infinite bandwidth and then applying a

ISBN 978-3-8007-6286-6 / ISSN 2197-4403

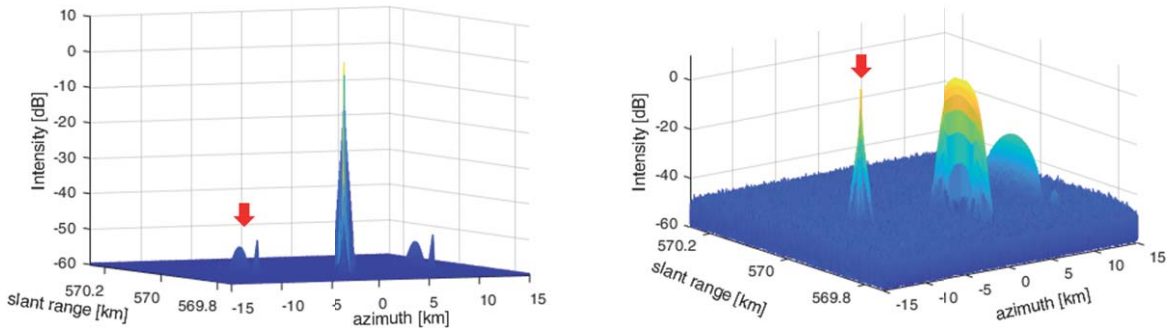

(a) (b)

Figure 4 Validation of derived ambiguity IRF. (a) Focused data. The first two ambiguities are shown in the plot, displaced by $\pm\Delta x_1$ from the main target. The intensity of the replica is attenuated by the antenna pattern and smeared in range and azimuth. (b) Focused ambiguity. Red markers point to the ambiguity that is refocused by the operator phase matched to (18).

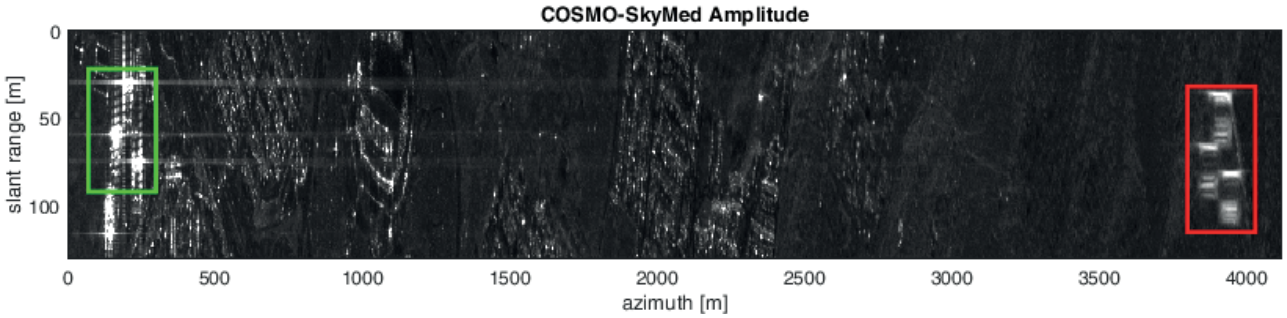

Figure 5 COSMO-SkyMed amplitude data acquired over Mexico. Strong targets (green) cause significant azimuth ambiguities (red), and the replicas are defocused. The data is represented in linear scale, and speckle reduction was obtained by temporal averaging of several images (for visualization only, the actual validation was performed with a single acquisition).

low-pass filter. The blurring in slant-range and azimuth domain for an infinite azimuth spectrum is:

$$\begin{aligned} &s^{\infty}_{i,def}(r,x) = \\ &\frac{1}{4\pi^2}\int_{-\frac{\pi}{dx}}^{\frac{\pi}{dx}} G_a(k_x+ik_{xs})e^{jk_x x}\left\{\int e^{jk'_r(r-iak_x)}dk'_r\right\}dk_x = \\ &\frac{1}{2\pi}\int_{-\frac{\pi}{dx}}^{\frac{\pi}{dx}} G_a(k_x+ik_{xs})e^{jk_x x}\delta\left(r-iak_x\right)dk_x = \\ &\frac{1}{2\pi ia}\int_{-\frac{\pi}{dx}}^{\frac{\pi}{dx}} G_a(k_x+ik_{xs})e^{jk_x x}\delta\left(\frac{r}{ia}-k_x\right)dk_x \end{aligned} \tag{11}$$

where the last transition exploits the scaling property of the Dirac delta function. The solution of (11) is:

$$\begin{aligned} &s^{\infty}_{i,def}(r,x) = \\ &\frac{1}{2\pi ia}G_a\left(\frac{r}{ia}+ik_{xs}\right)e^{j\frac{xr}{ia}}\,\mathrm{rect}\left(\frac{r}{ia\cdot k_{xs}}\right) \end{aligned} \tag{12}$$

Interestingly, the azimuth antenna pattern determines the ambiguity's amplitude pattern along the slant range. Moreover, it is clear that as the index i becomes larger, the amplitude decreases, limiting the effective number of ambiguities. The extent of the blurring in slant range also depends on the index i:

$$L_{i,r} = iak_{xs} = ir_0\left(\frac{\lambda}{2dx}\right)^2 \tag{13}$$

where $L_{r,i}$ is given in meters.
Next, we account for the finite bandwidth in range:

$$\begin{aligned} s_{i,def}(r,x) &= s^{\infty}_{def} * \left[B\,\mathrm{sinc}\left(\frac{r}{2\pi\rho}\right)\right] \\ &= \frac{B}{2\pi ia}G_a\left(\frac{r}{ia}+ik_{xs}\right)e^{j\frac{xr}{ia}} \\ &\quad\cdot\mathrm{rect}\left(\frac{r}{ia\cdot k_{xs}}\right)\mathrm{rect}\left(\frac{x}{ia\cdot 2\pi/\rho}\right) \end{aligned} \tag{14}$$

Thus, the extent of the ambiguity in the azimuth direction is:

$$L_{i,x} = i\frac{2\pi a}{\rho} = ir_0\frac{\lambda^2}{4d_x\rho} \tag{15}$$

Finally, we can summarize and formulate the complete IRF of the i-th azimuth ambiguity by combining (7), (8) and

ISBN 978-3-8007-6286-6 / ISSN 2197-4403

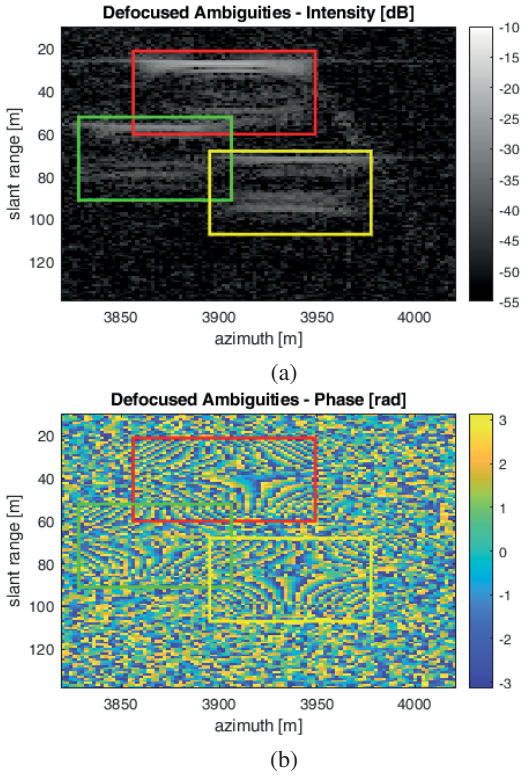

Figure 6 Azimuth ambiguities observed in COSMO-SkyMed SLC. (a) Intensity of the three ambiguous regions, each marked by a different color. (b) Phase of the ambiguities, resembling the hyperbolic paraboloid expected from (18).

(14) :

$$s_i(r,x) = A_i(r)e^{\psi_i(r,x)}\,\mathrm{rect}\left(\frac{r-\Delta r_i}{L_{i,x}}\right)\mathrm{rect}\left(\frac{x-\Delta x_i}{L_{i,r}}\right) \tag{16}$$

$$A_i(r) = \frac{B}{2\pi i a}G_a\left(\frac{r-\Delta r_i}{ia} + ik_{xs}\right) \tag{17}$$

$$\psi_i(r,x) = \frac{(x-\Delta x_i)(r-\Delta r_i)}{ia} + \frac{r_0(ik_{xs})^2}{2\Omega_0^2} \tag{18}$$

To visualize the structure of the result, we have simulated a point target observed by an X-band acquisition with the parameters from Table 1. The amplitude of the replica is demonstrated in Fig.2, following the relevant part of the antenna pattern. The phase is shown in Fig.3, shaped as the hyperbolic paraboloid predicted by (18).

3 Experimental Results

The presented model was tested on both the simulated X-band data and a real acquisition. First, we applied the operator phase matched to (18) to the ambiguity of the simulated point target. The operation should focus one of the ambiguities while blurring the true target. Indeed, Fig.4 confirms the expected behavior, validating the derived 2D ambiguity phase.

Further testing was conducted on a real COSMO-SkyMed acquisition over central Mexico in May 2019. The mission operates in X-band (9.6GHz) [9], and the pixel spacing of the image is 1m $\times$ 2m in slant range and azimuth, respectively. The amplitude of the data is shown in Fig.5, where a set of targets (marked in green) generates significant ambiguities (marked in red). Note that while the design of a SAR system should guarantee ambiguities to be negligible, the combination of strong backscatter from some targets and a weak response from the background can cause replicas to be visible.

As predicted by (7) and (8), ambiguities are shifted in both azimuth and slant range. Each replica is defocused, i.e., it is smeared over 39 pixels in slant range and 33 pixels in azimuth. Notice that the true targets are not isolated point scatterers but rather the combination of several targets along the azimuth direction (see Fig.7.a); thus, the observed smearing in the Single Look Complex (SLC) image (Fig.6.a) is wider than the calculated extent. While the smearing is almost uniform along the azimuth direction, it fluctuates along the slant range, following the relevant portion of the antenna pattern. The phase of the SLC image is shown in Fig.6.b, where the expected hyperbolic paraboloid can be appreciated.

As with the simulated data, we have focused the ambiguities by a convolution with the function phase matched to (14). The compression of ambiguities for COSMO-SkyMed data is shown in Fig.7.b. Comparing the focused result to the original scatterers (Fig.7.a), one can appreciate

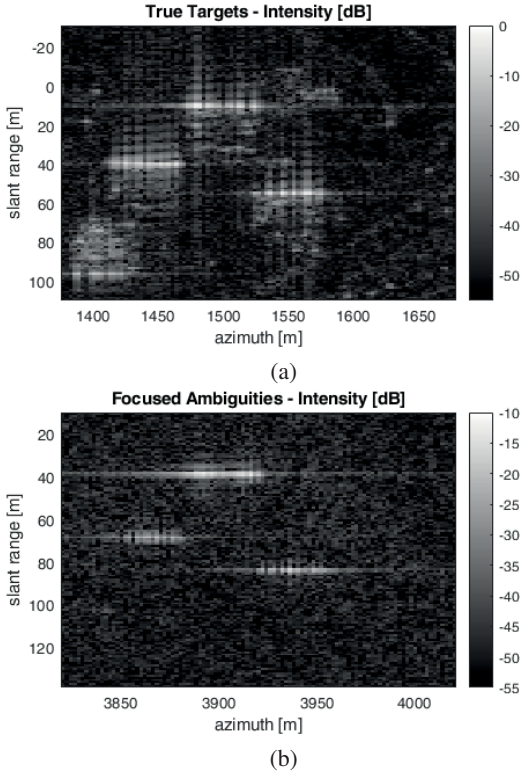

Figure 7 Intensity of COSMO-SkyMed data for: (a) True targets, where three lines of strong scatterers are evident. (b) Focused ambiguities. After the compression operation, we recovered the structure of the original data.

ISBN 978-3-8007-6286-6 / ISSN 2197-4403

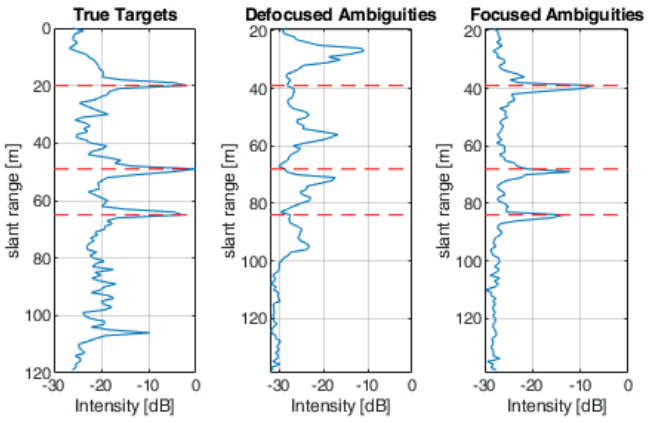

Figure 8 Range profile of COSMO-SkyMed data. Three major peaks are present in the true positions of the targets (left). The profile of the ambiguities in the SLC image is smeared due to defocusing (center). After refocusing (right), the peaks are recovered and shifted along range and azimuth.

that the spatial structure of the real targets was recovered, i.e., three lines along the azimuth direction.

The profiles along range are presented in Fig.8, obtained by averaging the relevant area over azimuth. In the position of the true targets, three distinct peaks are observed, corresponding to the three lines of strong scatterers in Fig.7.a. Azimuth ambiguities are defocused in the SLC data, and thus their profile along range is undecipherable, as shown in the middle figure. After refocusing we have obtained back the structure of the original signal, attenuated by the antenna pattern.

4 Conclusions

This work presents a complete 2D model of azimuth ambiguities, describing their position and spatial dispersion. By deriving the IRF of the replica in the focused data, we could precisely predict the replica's shape, which is very different from the original signal.

The proposed model was first tested by a simulated X-band SAR image, using a single point-target to verify the theoretical model. As an additional validation, a real COSMO-SkyMed acquisition was presented, where replicas of strong targets are noticeable. We demonstrated that applying the operator phase matched to the derived model makes it possible to refocus the ambiguity, validating its correctness.

Further studies are programmed to evaluate the model's applicability to ambiguity suppression algorithms and new parametric estimators.

5 Acknowledgments

We thank Prof. Fabio Rocca for his valuable advice. COSMO-SkyMed data, used for validating the derived ambiguity model, were provided within the ASI (Agenzia Spaziale Italiana) open call for science.

6 Literature

[1] F.k. Li and W.T.K. Johnson. Ambiguities in Spacebornene Synthetic Aperture Radar Systems. *IEEE Transactions on Aerospace and Electronic Systems*, AES-19(3):389–397, May 1983. Conference Name: IEEE Transactions on Aerospace and Electronic Systems.

[2] Michelangelo Villano and Gerhard Krieger. Spectral-Based Estimation of the Local Azimuth Ambiguity-to-Signal Ratio in SAR Images. *IEEE Transactions on Geoscience and Remote Sensing*, 52(5):2304–2313, May 2014. Conference Name: IEEE Transactions on Geoscience and Remote Sensing.

[3] Domenico Velotto, Matteo Soccorsi, and Susanne Lehner. Azimuth Ambiguities Removal for Ship Detection Using Full Polarimetric X-Band SAR Data. *IEEE Transactions on Geoscience and Remote Sensing*, 52(1):76–88, January 2014. Conference Name: IEEE Transactions on Geoscience and Remote Sensing.

[4] A.M. Guarnieri. Adaptive removal of azimuth ambiguities in SAR images. *IEEE Transactions on Geoscience and Remote Sensing*, 43(3):625–633, March 2005.

[5] Jie Chen, Mahboob Iqbal, Wei Yang, Peng-bo Wang, and Bing Sun. Mitigation of Azimuth Ambiguities in Spaceborne Stripmap SAR Images Using Selective Restoration. *IEEE Transactions on Geoscience and Remote Sensing*, 52(7):4038–4045, July 2014. Conference Name: IEEE Transactions on Geoscience and Remote Sensing.

[6] Jean-Paul Aguttes. Formations oriented along the path of SAR satellites, December 2003.

[7] R. Keith Raney and G. Julius Princz. Reconsideration of Azimuth Ambiguities in SAR. *IEEE Transactions on Geoscience and Remote Sensing*, GE-25(6):783–787, November 1987. Conference Name: IEEE Transactions on Geoscience and Remote Sensing.

[8] A. Moreira. Suppressing the azimuth ambiguities in synthetic aperture radar images. *IEEE Transactions on Geoscience and Remote Sensing*, 31(4):885–895, July 1993. Conference Name: IEEE Transactions on Geoscience and Remote Sensing.

[9] Andrea Torre, Diego Calabrese, and Manfredi Porfilio. COSMO-SkyMed: Image quality achievements. In *Proceedings of 5th International Conference on Recent Advances in Space Technologies - RAST2011*, pages 861–864, June 2011.

[10] R. Bamler. A comparison of range-Doppler and wavenumber domain SAR focusing algorithms. *IEEE Transactions on Geoscience and Remote Sensing*, 30(4):706–713, 1992.

ISBN 978-3-8007-6286-6 / ISSN 2197-4403